Desalination and Water Treatment
www.deswater.com

17 (2010) 57–65
May

1944-3994/1944-3986
doi: 10.5004/dwt.2010.1699

Multilayer ceramic deposition process of dense oxygen permeation membranes on porous supports

Y. Takahashi[a,b*], Y. Ando[b], A. Kawahara[b], M. Hirano[c], W. Shin[a,d]

[a]*Nagoya Institute of Technology, Department of Frontier Materials, Gokiso, Showa-ku, Nagoya, Aichi 466-8555, Japan*
Tel. +81561346215; Fax +81561344997; email: yosuke-takahashi@n.noritake.co.jp
[b]*Noritake Co., Limited, Research & Development Center, Development & Engineering Group, Miyoshi, Aichi 470-0293, Japan*
[c]*CHUBU Electric Power Co., Inc., Environmental Technology Group, Energy Applications R&D Center, Nagoya, Aichi 459-8522, Japan*
[d]*National Institute of Advanced Industrial Science and Technology, Nagoya, Aichi 463-8560, Japan*

Received 28 July 2009; accepted 7 December 2009

ABSTRACT

A multilayer ceramic deposition process of $La_{0.6}Sr_{0.4}Ti_{0.3}Fe_{0.7}O_{3-\delta}$ (LSTF) was developed for the fabrication of durable oxygen-permeable membranes. By optimizing the diameter of the starting powder and sintering temperature, defects such as peeling and cracking in the ceramic multilayer could be eliminated. With this optimized process, we have fabricated a thin membrane LSTF formed by the slurry coating process on porous support LSTF and found its rate of oxygen permeation to be 18 $cm^3/min/cm^2$. With this multilayer ceramic LSTF membrane, we have demonstrated the generation of oxygenated water with oxygen concentrations three times greater than that in water placed in ordinary atmosphere (32 mg/l).

Keywords: Ceramic membrane; $LaSrTiFeO_3$ perovskite oxide; Oxygen permeation

1. Introduction

Ceramic membrane reactors based on oxygen-ion conductors have drawn attention in recent years as a new technology for separating oxygen (O_2) from air. This technology with the ceramic membrane reactors allow low-cost on-site O_2 generation with smaller facilities, whereas a conventional cryogenic distillation plant requires the construction of massive facilities.

For the facilities/sites that require a relatively small volume of O_2, O_2 gas tanks delivered from an oxygen-generating facility are usually used. The ceramic membrane reactors allow the use of exhaust heat generated by the O_2 separating reaction as an auxiliary power source, for use in small facilities. This advantage allows the deployment of oxygen-permeable membranes not only to replace conventional oxygen-generating facilities but also to supply the by-product heat. For the application related to water oxygen-permeable membranes can also be used to generate oxygenated water, as shown in Fig. 1. The steam and inert gas flow on one side of the membrane-permeate-side and air flows on the other side of the membrane-air-side. The oxygen permeating the membrane dissolves in the steam, then after cooling, the oxygenated water is generated.

The ceramic membranes based on oxygen-ion-conductive ceramics induce dissociative absorption of oxygen molecules on the air side and transport oxide ions effectively using oxygen defects in the oxide, resulting in the recombination of oxide ions into

*Corresponding author

Presented at the Fifth Conference of the Aseanian Membrane Society Aseania 2009 "Recent Progress in Membrane Science and Technology", 12–14 July 2009, Kobe, Japan.

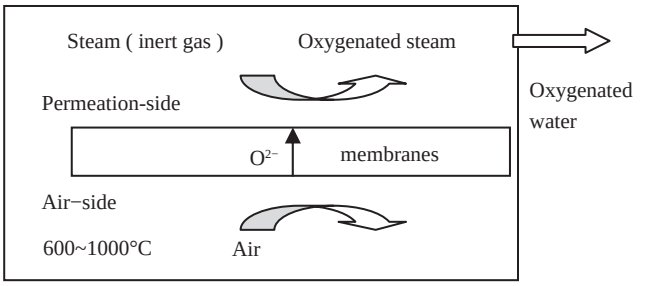

Fig. 1. Process of oxygenated water using oxygen permeation membranes.

oxygen molecules on the permeation side, which promotes oxygen permeation. The oxygen permeation becomes the rate-determining step for the oxygen ion conduction when membranes are thick. The surface reaction becomes the rate-determining step when membranes are thin. For the rate-determining step of oxygen ion conduction, the rate of oxygen permeation, j_{O2}, can be expressed by

$$j_{O2} = \left(RT \,/\, 16F^2L\right) * \sigma_i * \ln\left(PO_2^h \,/\, PO_2^l\right), \quad (1)$$

where R, T, F, L, σ_i, $PO_2{}^h$, and $PO_2{}^l$ are the gas constant, absolute temperature, Faraday constant, membrane thickness, oxygen ion conductivity, oxygen partial pressure on the air side, and oxygen partial pressure on the permeation side, respectively. According to Eq. (1), if the conditions of the oxygen permeation reaction (temperature, pressure) are fixed, the rate of oxygen permeation increases when materials with a higher oxygen ion conductivity or thinner membranes.

Two approaches have been used to enhance the O_2 permeation rate. The first is to develop new materials with high electronic and ionic conductivities. As it is well known, some perovskite-type oxides, $LaSrCoFeO_{3-\delta}$, $LaGaO_{3-\delta}$, and $BaSrCoFeO_{3-\delta}$, exhibit high electronic and ionic conductivities, as well as high oxygen permeability [1–8]. The second is to fabricate a very thin dense layer of oxygen-ion-conductive material on top of a porous support [9–11,13]. One factor impeding thin-membrane formation is the mismatch of the thermal expansion coefficient. Typical oxygen-ion-conductive ceramic membranes have large thermal expansion coefficients of 10–15 ($\times 10^{-6}/K^{-1}$) or greater, while the thermal expansion coefficient of porous ceramic supports (e.g., alumina) is around 5–7 ($\times 10^{-6}/K^{-1}$) [12–14]. This makes it difficult to use oxygen-ion-conductive ceramic membranes under the thermal cycle from R.T. to high temperatures. While one could use zirconia or magnesia, which have relatively high thermal expansion coefficients, such materials easily react with the membrane or degrade the membrane owing to the thermal shock resulting from the difference in thermal expansion coefficient. Researchers are currently exploring the fabrication of porous supports composed of the same material as the membranes, but this approach can give rise to other problems, including porosity deterioration and warping, as the supports undergo burning shrinkage when the membranes are heated to the densification temperature.

In this study, we have fabricated a novel membrane system composed of a dense and thin oxygen-ion-conductive layer and a multilayer porous support of the same material, changing the microstructure of each porous layer. We have developed novel durable oxygen-permeable membranes that do not cause any mechanical failure such as peeling, cracking, or deformation in the porous material by controlling the grain size of each porous layer.

We have investigated the properties of oxygen permeability of the membrane and demonstrated the oxygen permeation with our membrane system for water-related applications.

2. Experimental

2.1. Sample preparation

Fig. 2 shows the flowchart of the preparation of the ceramic membrane in this study. The starting material is an aqueous slurry of an oxide perovskite of a fixed composition of $La_{0.6}Sr_{0.4}Ti_{0.3}Fe_{0.7}O_{3-\delta}$ (LSTF) (average particle diameter: 1 μm). The slurry was sprayed and dried to obtain granulated powders with various particle diameters (A: 80 μm, B: 50 μm, C: 30 μm, D: 2 μm) by calcination processes. To predict the densification caused by the firing process, these powders were compacted into pellets (ϕ 25 mm × t 3 mm) using a compact press of 100 MPa, adding PVA aqueous solution. The pellets were fired at 1,400°C in air for 3 h. We evaluated the average pore size and porosity of the sintered bodies by the mercury penetration method.

Next, as listed in Table 1, we prepared samples with various support structures compacted into 25-mm-diameter pellets by applying a pressure of 100 MPa. We then screen-printed the paste (mixture of terpineol solvent and ethyl cellulose) prepared with powder D onto the top surface of the samples. By varying the viscosity of the paste and the number of screen-printing processes, we controlled the thickness of the printed membrane. The thickness of the membranes after drying ranged from approximately 0.1 to 0.5 mm. We fired these multilayer samples at 1,400°C in air atmosphere for 3 h to produce oxygen-permeable

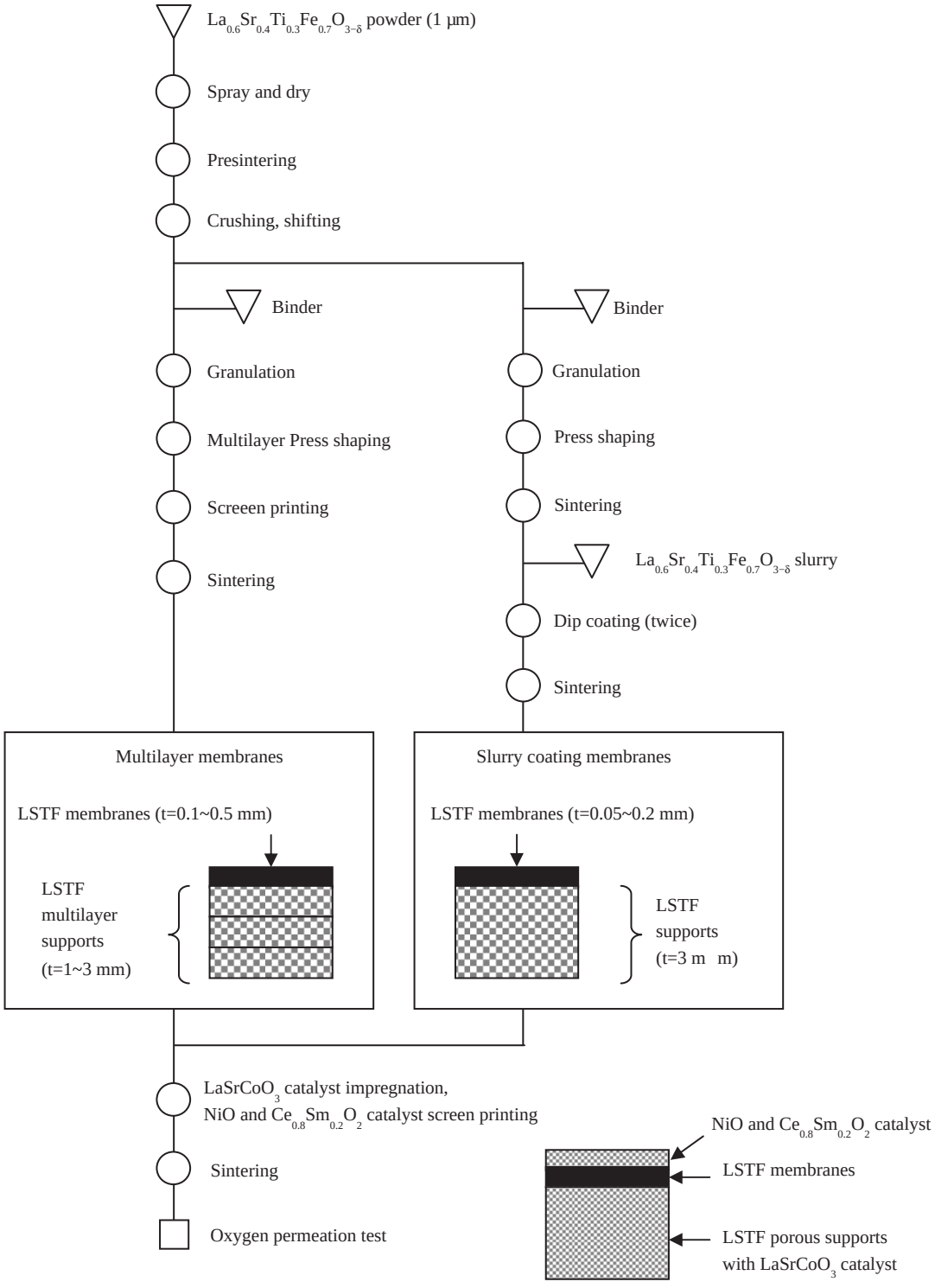

Fig. 2. Experimental flowchart.

membranes. For sample No. 4, this firing temperature was varied from 1,300°C to 1,450°C.

The thickness of the dense membrane was controlled by adjusting the number of repetitions of the slurry coating process. Powder compacts of (ϕ 25 mm $\times$ t 3 mm) pellets were prepared with powder A and a binder. The pellets were fired at 1,400°C in air for 3 h to prepare porous supports. The sintered supports were

Table 1
Fabrication of multilayer ceramic membrane

Sample	Porous support		Dense membrane (D)	
No.	Stacking	Thickness (mm)	*Process	Thickness (mm)
1	A	1	s.p	0.1, 0.2
2	A+C	2	s.p	0.3, 0.5
3	A+B	2	s.p	
4	A+B+C	3	s.p	
5	A	3	d	0.2
6	A	3	d	0.1
7	A	3	d	0.07
8	A	3	D	0.05

s.p = screen printing, d = dip coating

porous and the average pore diameter and porosity were 10 μm and 32%, respectively.

The slurry for coating was prepared with powder D (LSTF), xylene and a binder. A thick ceramic film was coated onto the porous support by dip coating and drying. The thickness of the film was controlled by the number of repetitions of dipping. Drying was carried out at 80°C for 30 min, and then, the sample was fired at 1,400°C in air for 3 h to prepare oxygen-permeable membranes.

To study the oxygen permeation performance of the samples, the electrode and catalyst were formed on the surface of the dense membrane. Also, an air electrode of $LaSrCoO_3$ was formed at the bottom of the porous support, as shown in Fig. 2.

A slurry made of mixed powder of NiO and $Ce_{0.8}Sm_{0.2}O_2$ with the mixing ratio of 1:1 by weight was screen-printed on top of the sample and dried. An organometallic solution of $LaSrCoO_3$ was screen-printed at the bottom of the sample and dried. The sample pellets were fired at 1,000°C for 1 h.

2.2. Characterization

The microstructures of the sintered oxygen-permeable membranes and porous supports were investigated using an SEM (JSM6490LA manufactured by JEOL) and a porosity meter (Auto Pore III manufactured by SHIMADZU) by the mercury penetration method. This method of using the high surface tension of mercury causes mercury to fill the pores in the sample. The specific surface area and porosity distribution are then determined from the applied pressure and the amount of infiltrated mercury.

Fig. 3 shows the oxygen-permeable membrane evaluation equipment. The sample placement section was constructed by placing a pellet of the oxygen separation membrane between two high-density alumina tubes and joining them with glass.

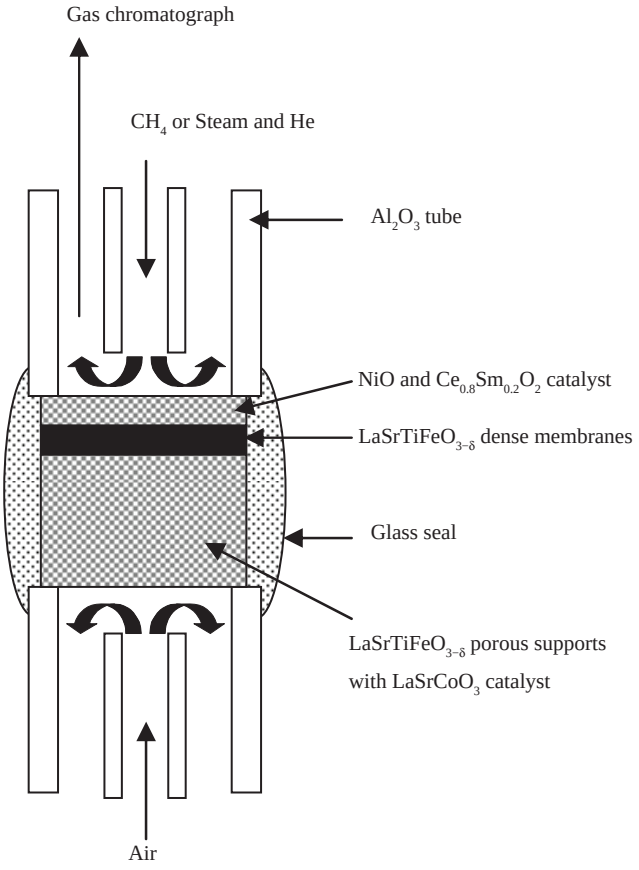

Fig. 3. Experimental setup for oxygen permeation of the membranes.

At temperatures between 800°C and 1,000°C, we supplied air to the air electrode side and fuel gas of CH_4 or helium gas mixed with water vapor to the fuel electrode side. The CH_4 supplied to the fuel electrode side reacted with the oxygen permeating the oxygen separation membrane near the fuel electrode catalyst ($CH_4 + 1/2O_2 \rightarrow 2H_2 + CO$), generating a synthesis gas ($H_2 + CO$). The rate of oxygen permeation was calculated from the flow rate for each gas and the concentration of oxygen or synthesis gas analyzed at the fuel-side flow. The gas was analyzed with a gas chromatograph (GL science CP-4900). The volumetric ratio of the nitrogen contained in the entire fuel electrode emission gas was defined as the nitrogen leak ratio.

3. Results and discussion

Fig. 4 shows the SEM images of the raw powders A, B, C, and D and of the sintered bodies after sintering. Dense microstructures could be obtained with the starting powder of smaller particle size.

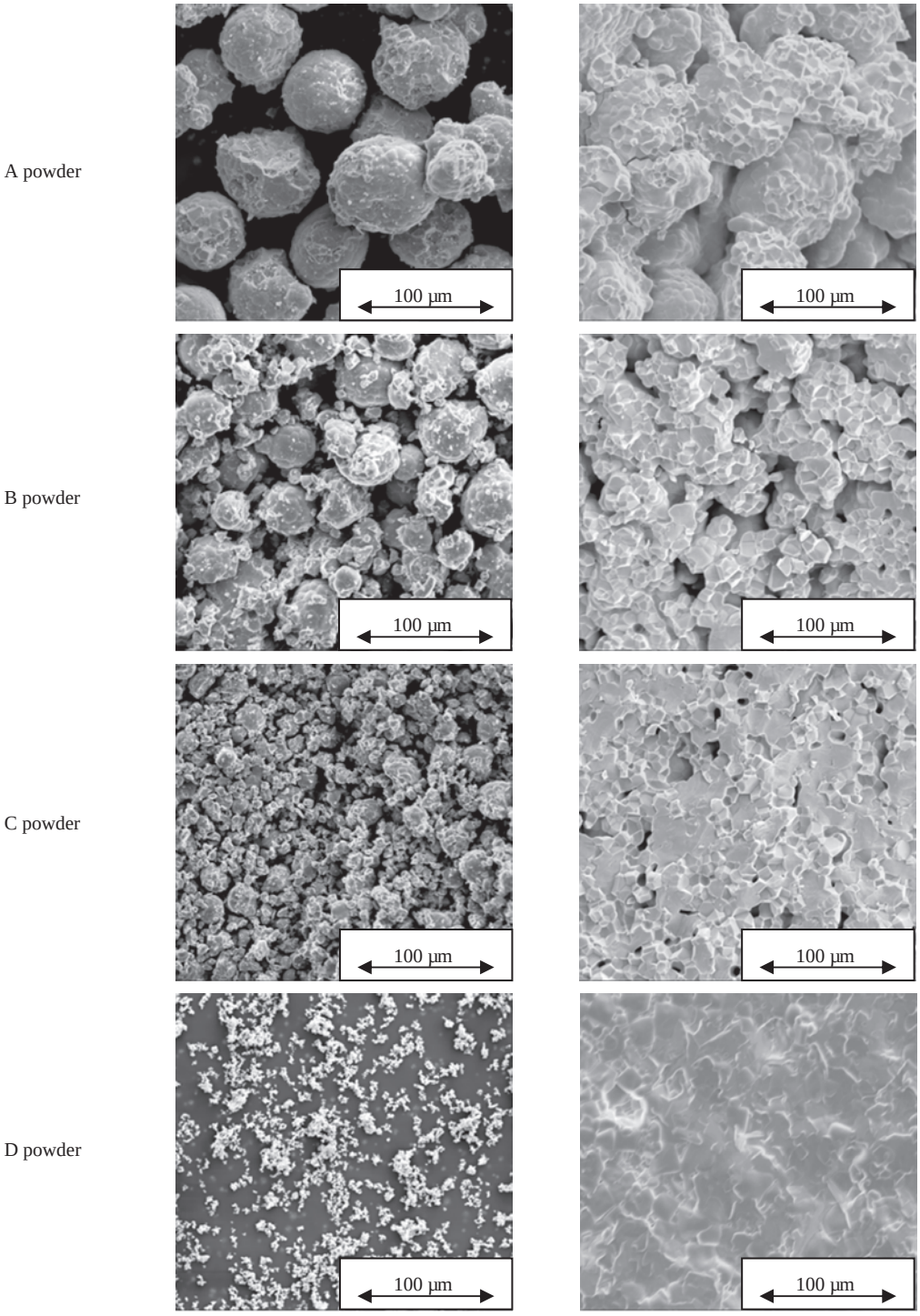

Fig. 4. SEM image of (a) LSTF powder and (b) after sintering.

The finest powder D resulted in the highest density in the sintered body. From these results, powder D was chosen for the preparation of dense oxygen-permeable membranes.

After sintering, numerous defects involving peeling at layer boundaries were found in sample No. 1. We attribute these flaws to the stress induced by the large difference in shrinkage rate between the support and the

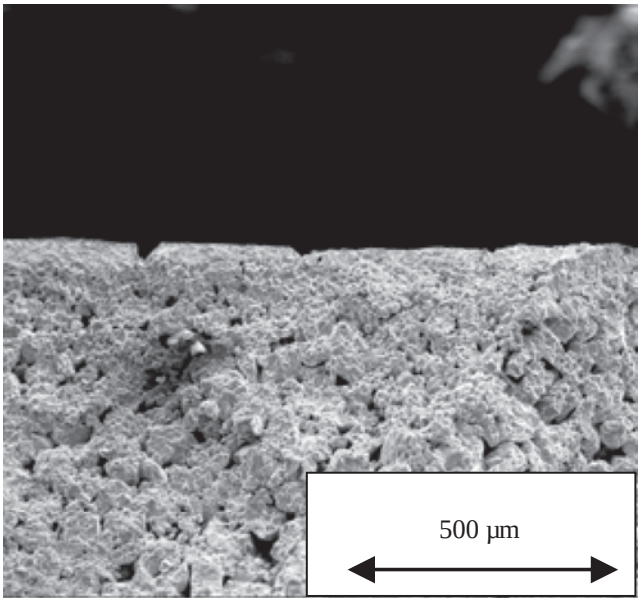

Cross section

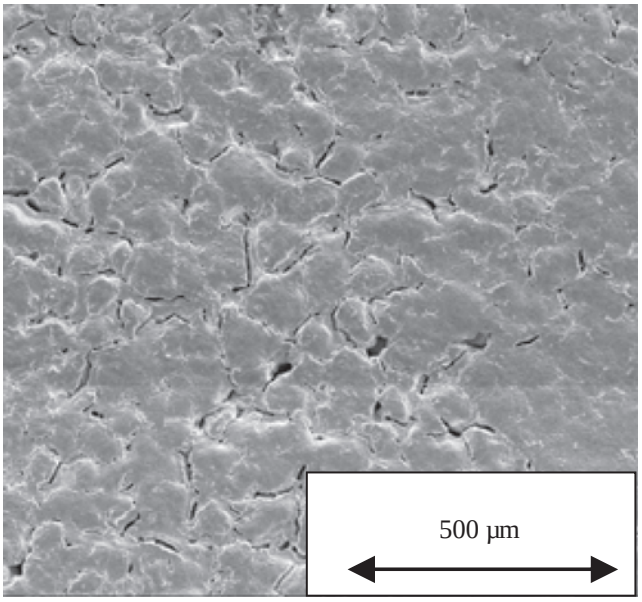

Membrane surface

Fig. 5. SEM image of $La_{0.6}Sr_{0.4}$ $Ti_{0.3}Fe_{0.7}O_{3-\delta}$ membrane 2 sintering at 1,400°C.

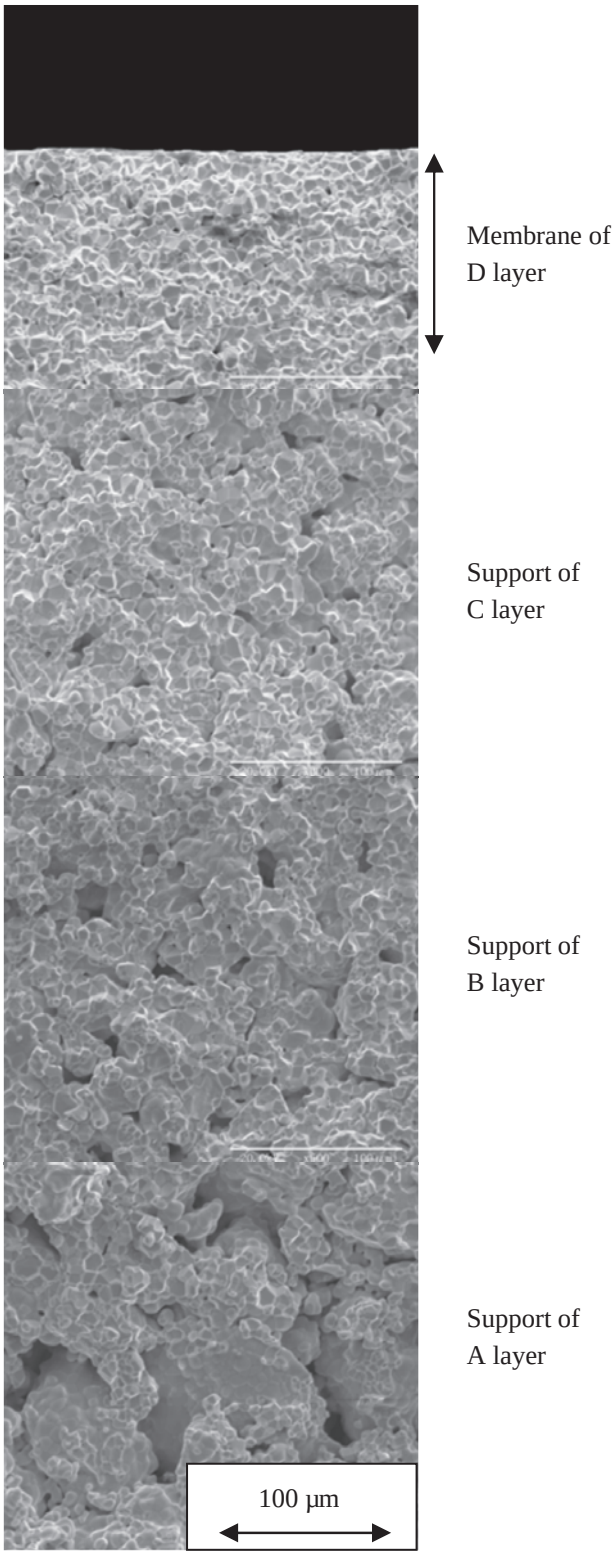

Fig. 6. Cross section SEM image of $La_{0.6}Sr_{0.4}$ $Ti_{0.3}Fe_{0.7}O_{3-\delta}$ membrane 4 sintering at 1,400°C.

Table 2
Data of the microstructure of the sintered body in each layer

Starting powder/Average grain diameter of starting powder (μm)	1,400°C sintered average pore diameter (μm)	1,400°C sintered porosity (%)	1,400°C sintered shrinkage (%)
A/80	10	32	7
B/50	5.8	17	10
C/30	1.5	5	15
D/≤10	≤0.5	≤2	20

Table 3
Frequency of defect in the 20 samples prepared

Sample No.	1	2	3	4	5	6	7	8
Frequency of peeling and cracking for membranes	90%	20%	30%	0%	90%	70%	40%	30%
Frequency of bending for supports	5%	20%	10%	5%	30%	10%	10%	10%
				1400°C sintered				

membrane during firing. No peeling occurred in samples No. 2 and 3, but a large deformation resulted, causing many cracks on the surface of the membrane, as shown in the SEM image in Fig. 5. We suspect that the double-layer structure of the supports of samples No. 2 and 3 reduced the difference in shrinkage rate during firing.

The membranes with the particle-size-graded structure could reduce the stress induced by the different shrinkage behaviors. Sample No. 4 exhibited no peeling or cracking (Fig. 6). Table 2 shows the data of the microstructure of the sintered body in each layer. Table 3 shows the frequency of defect formation in the 20 samples prepared. We obtained the best results in sample No. 4, which featured the particle-size-graded structure. On the basis of the results in Tables 2 and 3, the difference between the shrinkage rates of the membrane and support should be below 10% to prohibit any unwanted defects.

Fig. 7 shows SEM images of the surfaces of the sample No. 4 fired at different temperatures from 1,300°C to 1,400°C. Firing at 1,300°C generated a relatively large number of pores. Firing at 1,350°C and higher resulted in a dense structure. At 1,450°C, grain growth occurred.

Fig. 8 shows the oxygen permeation of the membranes of No. 4 sintered at different temperatures, investigated under methane reforming conditions. The sample fired at 1,300°C exhibited a low density and appreciable nitrogen leakage, and its rate of oxygen permeation was low. The dense sample fired at 1,400°C showed a high rate of oxygen permeation: 12 $cm^3/min/cm^2$. For the sample fired at 1,450°C, the rate of nitrogen leak was about the same as that of the sample fired at 1,400°C, but its oxygen permeability was lower. We hypothesize that the oxygen permeability of the sample fired at 1,400°C is degraded by decreased ion conductivity in areas where sectional grain growth occurred.

By the slurry coating process, a very thin and dense membrane with a thickness of 50 μm was prepared (Fig. 9). As shown in Table 3, a thinner oxygen-permeable membrane was confirmed to exhibit a lower frequency of defects generation such as membrane

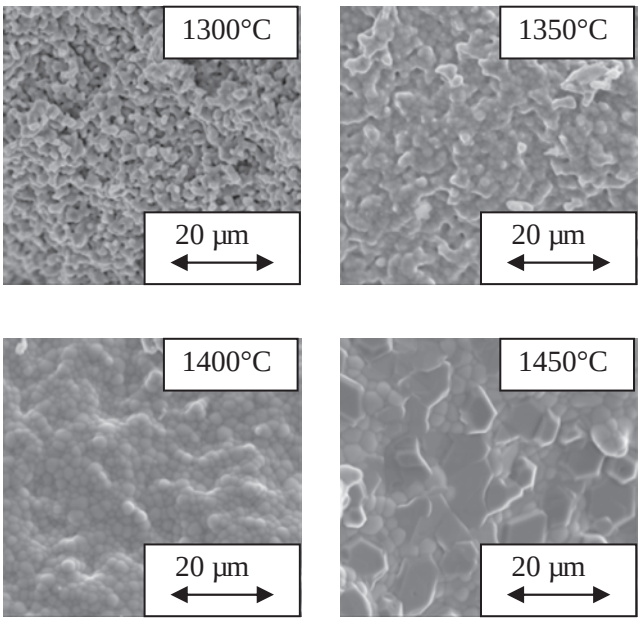

Fig. 7. SEM image of $La_{0.6}Sr_{0.4}$ $Ti_{0.3}Fe_{0.7}O_{3-\delta}$ membrane 4 sintering at 1,300–1,450°C.

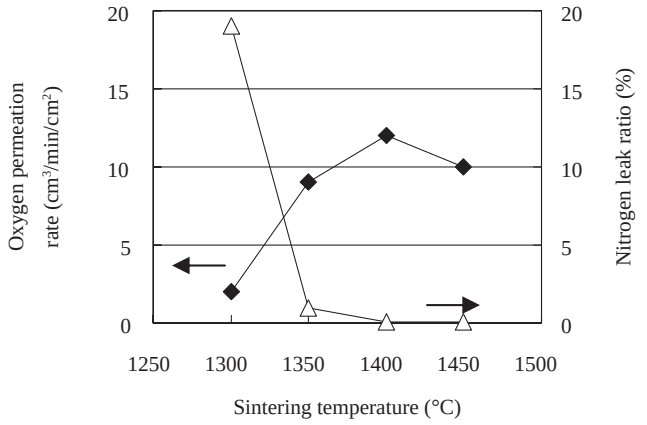

Fig. 8. Temperature dependence of oxygen permeation rates and nitrogen leak ratio for $La_{0.6}Sr_{0.4}Ti_{0.3}Fe_{0.7}O_{3-\delta}$ membrane 4. (CH_4/Membranes/Air 1,000°C).

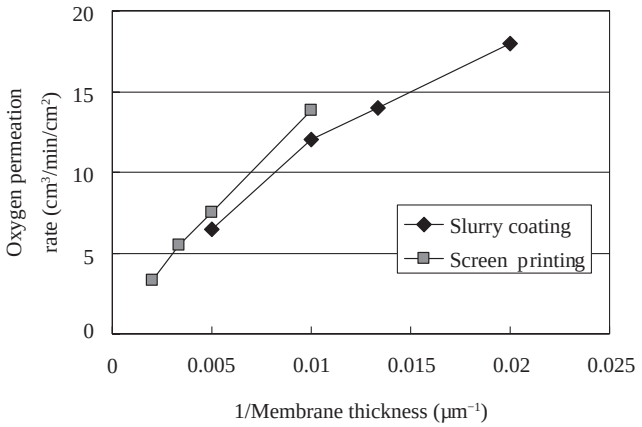

Fig. 10. Relationship between the reciprocal of membrane thickness and oxygen permeation rates for LSTF oxygen membranes prepared by the screen printing process and slurry coating process. (CH_4/Membranes/Air 1,000°C).

cracking, peeling, and warping of the support. We believe that this is attributable to the large shrinkage observed in the lateral direction of the membrane cross section and the lack of any mitigation of this stress. With the thin membrane formed by the slurry coating process, we successfully improved the rate of oxygen permeation to 18 $cm^3/min/cm^2$. This increase in permeation performance is attributable to the reduced thickness of the membrane, which increased the ion conduction across the membrane thickness.

Fig. 10 indicates the relationship between the reciprocal of membrane thickness and the rate of oxygen permeation of the LSTF oxygen-permeable membranes prepared by the screen printing and slurry coating processes. The rate of oxygen permeation increased proportionally to the reciprocal of membrane thickness, but the gradient declined in thin-membrane regions. The deviation from the theoretical value derived from Eq. (1) was greater in thin-membrane regions. In other words, other factor than the conductivity of ions in the membrane seems to cause limiting effects. One reason is insufficient catalyst activity due to inadequately supported catalyst particles in the support near the membrane. In short, an increase in the amount of permeated oxygen appears to have functioned as a limiting factor in surface reactions between the membrane and the catalyst boundary surface. Another possible cause is the factor that limits gas diffusion within the support.

Comparing the multilayer and slurry coating processes, we determined that membranes formed by the

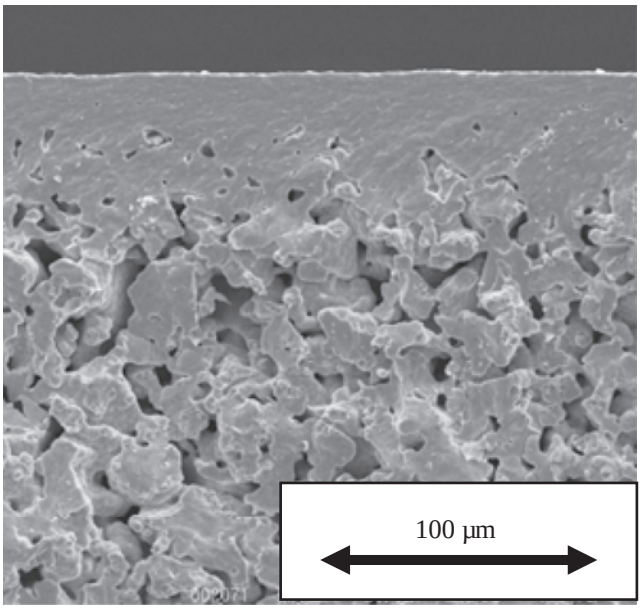

Fig. 9. SEM image of $La_{0.6}Sr_{0.4}Ti_{0.3}Fe_{0.7}O_{3-\delta}$ membranes by slurry coating process.

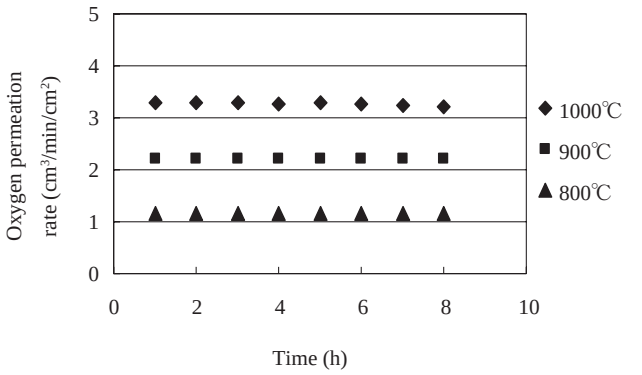

Fig. 11. Time course of oxygen permeation rates for LSTF membranes at various temperature. (He+Steam/Membranes/Air).

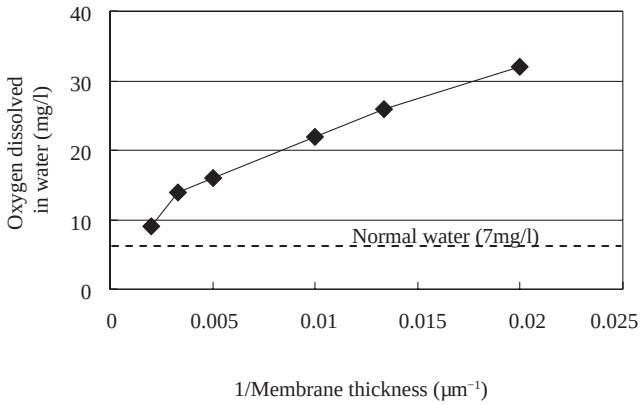

Fig. 12. Relationship between the reciprocal of membrane thickness and concentrations of oxygen dissolved in water.

slurry coating process, which enables the creation of thinner membranes, provide a higher oxygen permeability. However, when the membrane and support are made of the same material, as in our experiments, the frequency of defects generated by shrinkage resulting from firing was significantly low. For future industrial applications, we recommend the combination two processes: the formation of a membrane by the slurry coating process on a support prepared by the multilayer process.

We performed an evaluation with water vapor and helium gas/membrane/air (membrane thickness: 0.5 mm) to assess the durability in a water-related application. Fig. 11 shows the results of this evaluation. Oxygen permeability remained at 97% or above after eight hours under temperatures of 800°C, 900°C, and 1,000°C, indicating an adequate basic durability in water-related processes.

Fig. 12 shows the relationship between the reciprocal of membrane thickness and the concentration of oxygen dissolved in water. For the membranes with high oxygen permeability, concentrations of dissolved oxygen were also high. From this result, we deduce that improving the performance of oxygen-permeable membranes increases the productivity of a high-concentration oxygenated water manufacturing process. The concentrations of oxygen dissolved in the oxygenated water obtained in our experiments were 32 mg/l more than three times greater than oxygen concentrations in water placed in ordinary atmosphere and approached oxygen concentrations in commercially available high-concentration oxygenated water products. In environments where exhaust heat is available, it is suggested that using ceramic oxygen-permeable membranes offers a practical way to generate high-density oxygenated water.

4. Conclusions

A multilayer ceramic deposition process of LSTF was developed for the fabrication of durable oxygen-permeable membranes. By optimizing the diameter of the starting powder and sintering temperature, defects such as peeling and cracking in the ceramic multilayer could be eliminated. The diameter of the starting powder particles for the membrane and the sintering temperature were 2 μm and 1,400°C, respectively. The difference between the shrinkage rates of the membrane and the support should be below 10%. With this optimized process condition, we fabricated a thin LSTF membrane formed by the slurry coating process on porous support LSTF and found its rate of oxygen permeation to be 18 $cm^3/min/cm^2$. With this multilayer ceramic LSTF membrane, we have demonstrated the generation of oxygenated water with oxygen concentrations three times greater than that in water placed in ordinary atmosphere (32 mg/l).

References

[1] Y. Teraoka, H.M. Zhang, K. Okamoto and N. Yamazoe, Mat. Res. Bull., 23 (1988) 51–58.
[2] Y. Teraoka, H.M. Zhang, S. Furukawa and N. Yamazoe, Chem. Lett., (1985) 1743–1746.
[3] Y. Teraoka, Y. Honbe, J. Ishii, H. Furukawa and I. Moriguchi, Solid State Ionics, 152–153 (2002) 681–687.
[4] T. Ishihara, H. Matsuda and Y. Takita, J. Am. Chem. Soc., 116 (1994) 3801–3803.
[5] T. Ihshihara, Catal. Soc. Japan, 45(3) (2003) 263–268.
[6] Y. Tsuruta, T. Todaka, H. Nishiguchi and T. Ishihara, Electrochem. Solid-State Lett., 4(3) (2001) E13–E15.
[7] Z. Shao, W. Yang, Y. Cong, H. Dong, J. Tong and G. Xiong, J. Membr. Sci., 172 (2000) 177–188.
[8] Z. Shao, H. Dong, G. Xiong, Y. Cong and W. Yang, J. Membr. Sci., 183 (2001) 181–192.
[9] Y. Teraoka, T. Fukuda, N. Miura and N. Yamazoe, J. Ceram. Soc. Japan, 97(4) (1989) 476–472.
[10] Y. Teraoka, T. Fukuda, N. Miura and N. Yamazoe, J. Ceram. Soc. Japan, 97(5) (1989) 533–538.
[11] S. Hamakawa and F. Mizukami, Catal. Soc. Japan, 48(5) (2006) 308–313.
[12] L.W. Tai, M.M. Nasrallah, H.U. Anderson, D.M. Sparlin and S.R. Sehlin, Solid State Ion., 76 (1995) 273–283.
[13] E.A.F. Span, F.J.G. Roesthuis, D.H.A. Blank and H. Rogalla, Appl. Phys. A, 69 (1999) 783–785.
[14] H. Kurimura and M. Harada, Membrane, 29(5) (2004) 265–271.